THE UNIVERSITY of EDINBURGH

Edinburgh Research Explorer

Flame extension lengths beneath a confined ceiling induced by fire in a channel with longitudinal air flow

Citation for published version:
Qiu, A, Hu, L, Chen, L & Carvel, RO 2018, 'Flame extension lengths beneath a confined ceiling induced by fire in a channel with longitudinal air flow', *Fire Safety Journal*, vol. 97, pp. 29-43. https://doi.org/10.1016/j.firesaf.2018.02.003

Digital Object Identifier (DOI):
10.1016/j.firesaf.2018.02.003

Link:
Link to publication record in Edinburgh Research Explorer

Document Version:
Peer reviewed version

Published In:
Fire Safety Journal

General rights
Copyright for the publications made accessible via the Edinburgh Research Explorer is retained by the author(s) and / or other copyright owners and it is a condition of accessing these publications that users recognise and abide by the legal requirements associated with these rights.

Take down policy
The University of Edinburgh has made every reasonable effort to ensure that Edinburgh Research Explorer content complies with UK legislation. If you believe that the public display of this file breaches copyright please contact openaccess@ed.ac.uk providing details, and we will remove access to the work immediately and investigate your claim.

OPEN ACCESS

Download date: 12. Oct. 2024

Flame extension lengths beneath a confined ceiling induced by fire in a channel with longitudinal air flow

Ang Qiu[a], Longhua Hu[a]*, LongFei Chen[a], Ricky O. Carvel[b]

[a] State Key Laboratory of Fire Science,
University of Science and Technology of China,
Hefei, Anhui, 230026, China

[b] BRE Centre for Fire Safety Engineering
The School of Engineering, University of Edinburgh, UK

*Corresponding author: Tel: (86) 551 63606446; Fax: (86) 551 63601669; Email address: hlh@ustc.edu.cn; Postal address: State Key Laboratory of Fire Science, University of Science and Technology of China, Hefei, Anhui, 230026, China.

Abstract

This paper investigates the length of flame extension for an impinging flame underneath the confined ceiling in a channel with longitudinal air flow. Previous works in this field have been primarily concerned with un-confined ceilings and no forced air flow conditions. Under longitudinal air flow conditions, the flame extension beneath the channel ceiling is non-symmetrical, that is, different in the upstream and downstream directions from the fire source. In this study, experiments were carried out with two channeled ceilings with widths of 1.5 m and 0.5 m. Square porous gas burners of different sizes were employed as the fire source, using propane as fuel, with various heat release rates and source-ceiling heights. The flame extension lengths beneath the ceiling, both upstream and downstream from the fire source, were measured. Their difference as well as their total length was quantified for different magnitudes of forced longitudinal air flow along the channel. Results show that the flame extension lengths beneath the ceiling increases with heat release rate, but decreases with source-ceiling height, channel width, burner size or longitudinal air flow speed. With a longitudinal air flow, the flame extension is longer downstream than upstream. Non-dimensional correlations are proposed for the flame extension lengths (upstream, downstream and their total length), based on the unburnt fuel distribution upstream and downstream, as well as considering air entrainment of the ceiling flow, which further consumes the unburnt fuel along the ceiling. These correlations are shown to fit the data well.

Key words: flame extension length; confined ceiling; longitudinal air flow; source-ceiling height; heat release rate; channel fire.

Nomenclature

c_p	specific heat of air at constant pressure (kJ/kg•K)
d	depth of hot gas layer beneath corridor ceiling (m)
D	diameter of fire source/side dimension of square burner (m)
g	gravitational acceleration (m/s^2)
H	source-ceiling height (m)
H_f	free flame height (m)
ΔH_∞	heat released per kg of air consumed (kJ/kg)
ΔH_{fuel}	heat of combustion of the fuel (kJ/kg)
l_f	flame length beneath the corridor ceiling(m)
l_{fe}	flame extension length along the channel ceiling (m)
$l_{fe,0}$	flame extension length beneath the channel ceiling with no air flow (m)
$l_{fe,upstream}$	flame extension length beneath the channel ceiling for the upstream with air flow (m).
$l_{fe,downstream}$	flame extension length beneath the channel ceiling for the downstream with air flow (m).
Q	heat release rate (kW)
r_f	radical flame extension length beneath ceiling (m)
T_∞	ambient air temperature (K)
ΔT_f	flame temperature rise above ambient air temperature (K)
u_a	longitudinal air flow speed (m/s)
u_e	characteristic velocity of the ceiling flow after impingement (m/s)
V_{fuel}	fuel volume flow rate (m^3/s)
W	channel width (m)

Greek symbols

ρ_∞	ambient air density (kg/m^3)
$\Delta\rho_f$	density difference between flame and ambient air (kg/m^3)
θ	flame tilt angle (degree)

Subscripts	
fe	flame
p	constant pressure
∞	ambient

1. Introduction

When the free flame height of a fire is higher than the ceiling height, the flame impinges upon the ceiling and extends for some distance beneath the ceiling. This impinging flame will result in a very high heat flux to the ceiling and an enhanced radiative flux to the lower parts of the surrounding environment [1-3]. This high heat flux may have a significant effect on any combustible materials leading to further ignition, and may also cause physical damage to non-combustible materials. So, the flame extension length beneath the ceiling is an important parameter to be quantified and modeled. The behavior of the impinged flame may be divided into two broad scenarios: (i) for an unconfined ceiling where the flame extends radially in an axi-symmetrical manner; or (ii) for a confined ceiling, for example, in a long-narrow structure (such as a corridor, tunnel or duct), where the flame is constrained by the side walls and extends along the ceiling in two opposite directions from the fire source.

For the flame extension length beneath an unconfined ceiling, You and Faeth [1] proposed an empirical correlation, which is widely used in practice:

$$r_f \big/ D = 0.502\left[\left(H_f - H\right)\big/ D\right]^{0.957} \tag{1}$$

where r_f is the radial flame extension length beneath ceiling; H_f is the visible flame height (free burning, without the ceiling); H is the source-ceiling height; and D is the diameter of the fire source. Babrauskas [2] reviewed the problem in 1980s. Gross [3] obtained some data with 0.61 m and 0.91 m diameter burners (104-283 kW). Hasemi and Yokobayashi [4] proposed following formula

based on a dimensionless fire heat release rate:

$$r_f / D = 2.58 Q^{*2/5} (H/D)^{2/5} - H/D \tag{2}$$

with

$$Q^* = \frac{Q}{\rho_\infty T_\infty c_p g^{1/2} D^{5/2}} \tag{3}$$

where Q is the heat release rate; ρ_∞ is the ambient air density; T_∞ is the ambient air temperature; c_p is specific heat capacity of air at constant pressure; and g is the acceleration due to gravity. The data in [4] was further correlated non-dimensionally [5] using source-ceiling height *H* for normalization rather than source dimension *D*. Ding and Quintiere [6] also proposed another non-dimensional correlation based on a theoretical analysis to predict the flame extension length beneath the ceiling using source dimension *D* for normalization:

$$r_f / D = 1.62 Q^{*2/5} \tag{4}$$

More recently, Zhang et al. [7, 8] proposed correlations of flame extension lengths beneath an un-confined ceiling induced by round jet fires, as well as beneath an un-confined inclined ceiling by rectangular-source fires.

For the flame extension behavior beneath a confined ceiling (for example in a corridor), the studies are somewhat limited. Hinkley [9, 10] measured the heat flux to the ceiling due to flame impingement in a 1.2 m wide corridor with a gas burner located at the end of the corridor, for a range of heat release rates (170-600 kW) and the burner at various distances (0.37-1.20 m) below the ceiling. Following formula was proposed [9, 10] to predict the flame length beneath the corridor ceiling for above scenario:

$$l_f = 2.2 \left(\frac{m'}{\rho_\infty g^{1/2} d} \right)^{2/3} \tag{5}$$

where l_f is the flame extension length; m' is the flow rate of fuel per unit width of corridor; and d is the thickness of hot gas layer beneath the corridor ceiling.

It should be noted that limited research has been carried out on the flame extension behavior in a long-narrow structure with an imposed air flow. These situations commonly exist in the real world, for example in a transportation tunnel where longitudinal forced ventilation is usually employed for pollution or smoke control [e.g., 11-16]. Even in corridors inside buildings, longitudinal flows may exist. For example, a smoke extraction system installed in the ceiling at one end of a corridor may induce such longitudinal air flow along the corridor, through an opening (window) at the other end. With such air flow, the flame extension length beneath the confined ceiling in a channel or corridor will be unsymmetrical, that is, different in the upstream and the downstream directions from the fire source. However, this asymmetry has not been well quantified to date. Recently, Ingason and Li [17-20] studied the flame length in longitudinally ventilated tunnels. In those works, flame extension lengths are defined as the distance between the flame tip and the center of the fire source. For fires with flames not reaching the ceiling at relatively higher longitudinal ventilation, the horizontal lengths of the inclined flames are estimated and used as the downstream flame lengths. The normalized flame lengths by the tunnel height, $\frac{l_f}{H}$, were correlated against a non-dimensional heat release rate defined as $\frac{Q}{\rho c_p T_0 \sqrt{g} A H_{ef}^{1/2}}$,where l_f is the flame length, H is the tunnel height, Q is the heat release rate, H_{ef} the source-ceiling height, ρ is the ambient air density, c_p is the specific heat of air at constant pressure, T_0 is the ambient air temperature and A is the cross-sectional area of the tunnel. In [18], the major finding and conclusion is that the flame length (downstream in [18]) is un-affected by the longitudinal ventilation velocity. It is noted that in these works, the data investigated is from relatively

large scale fire tests (like the HGV-EUREKA 499 fire test [21], the Memorial Tests [22] and Lönnermark and Ingason [23]), that the longitudinal ventilation is relatively weak and its effect on the flame length might be not obvious.

This paper presents comprehensive experiments which were carried out in a channel with two different channeled ceiling widths to measure the flame extension lengths beneath the confined ceiling, both upstream and downstream, as well as the total flame extension length. This was tested with longitudinal air flows, for various heat release rates, channel widths and source-ceiling heights. Relatively small fires were employed, for which the flame extension length is very sensitive to the longitudinal ventilation velocity. The design of these scenarios is to highlight the effect of longitudinal ventilation on the flame extension length beneath the ceiling in tunnel fires. The data is analyzed using a different methodology, which is performed based on the physics of the unburnt fuel distribution upstream and downstream, as well as considering air entrainment of the ceiling flow which further consumes the unburnt fuel along the ceiling. According to the analysis, non-dimensional correlations are proposed for the flame extension lengths (upstream and downstream as well as their total length).

2. Experimental

Figure 1 shows the experimental setup. Experiments were carried out in a 72 m long channel [24] with two different channeled ceiling widths (0.5 m and 1.5 m respectively, as shown in Fig. 1b). The longitudinal air flow through the channel was generated by a mechanical fan and screened at one end of the channel [25]. The ceiling of the channel is lined with mica board (2 cm thickness) with low thermal conductivity of 0.035 W/(m·K) and good thermal resistance performance. The side walls of the channel are constructed of fire-proof glass in order to record the flame position, using a CCD video camera.

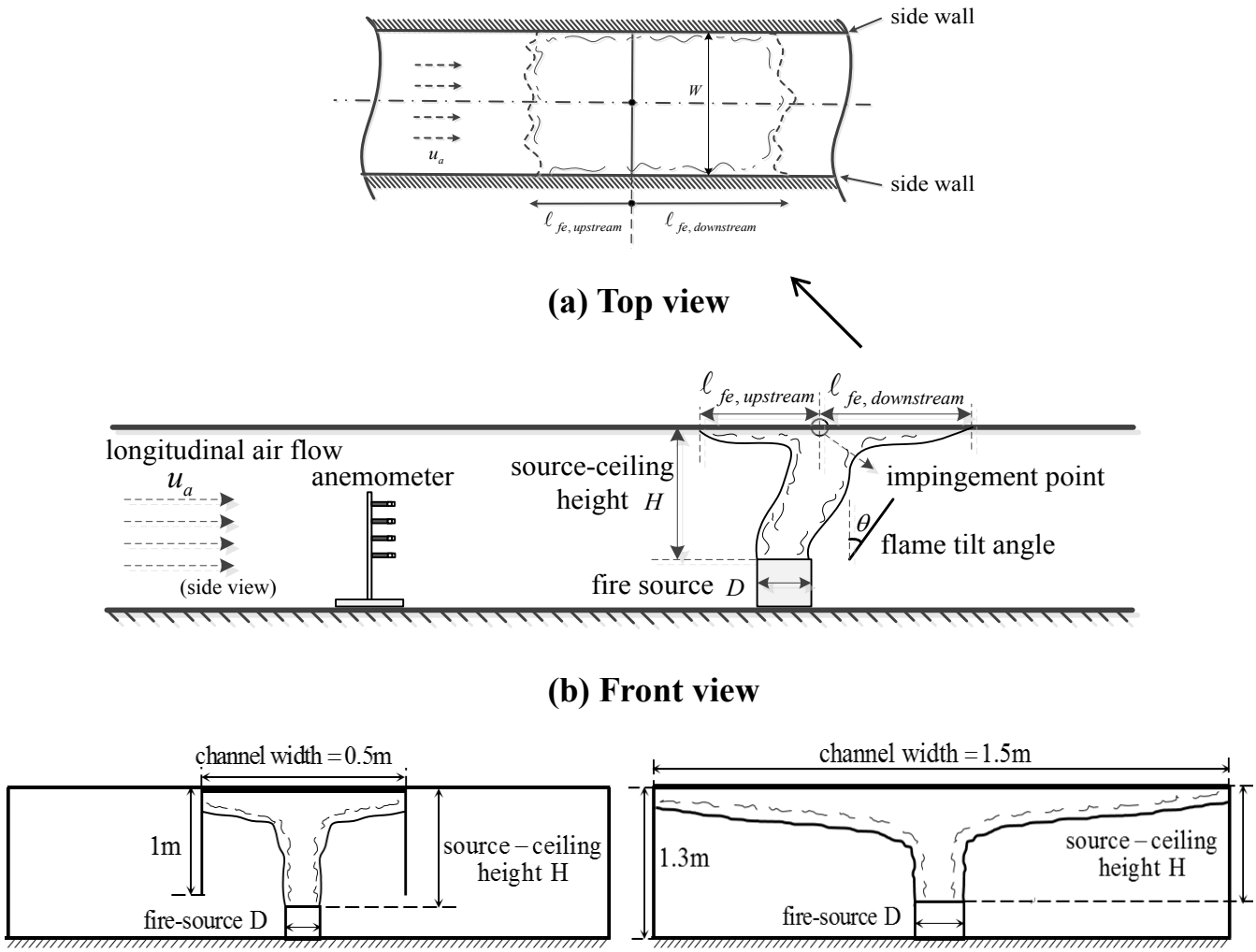

Fig. 1 Experimental setup

Square porous gas burners (with side dimensions of 15 cm and 20 cm for the 0.5 m wide channel; with side dimensions of 25 cm, 30 cm and 35 cm for the 1.5 m wide channel) made of stainless steel and with many small holes distributed evenly across the surface, were used as the fire source. The gaseous burners were positioned at 85 cm, 90 cm or 95 cm above the channel floor, to give three source-ceiling heights (45 cm, 40 cm and 35 cm). Propane was used as fuel with supply rates controlled by a gas flow meter, and the corresponding heat release rates were calculated based on the heat of

combustion of the fuel. Gaseous fuel, rather than liquid fuel (for example, pool fire) or solid fuel (for example, wood crib), was used in order to generate steady fire heat release rates, which would not be affected by variations in the longitudinal air flow. The heat release rate (HRR) tested were 51.0 kW, 61.2 kW, 71.4 kW, 81.6 kW, 91.8 kW, 102.3 kW, 112.2 kW, 122.4 kW, 132.6 kW, 142.8 kW, and 153.1 kW when the channel ceiling width was 0.5 m; and were 130 kW, 140 kW, 150 kW, 160 kW, 170 kW, 200 kW, and 220 kW when the channel ceiling width was 1.5 m.

Four levels of longitudinal air flow speeds were considered: 0 m/s, 0.3 m/s, 0.5 m/s and 0.8 m/s in the 1.5 m wide channel; and 0 m/s, 0.6 m/s, 1.2 m/s, and 1.8 m/s in the 0.5 m wide channel. At higher longitudinal air flow speeds than these, the flame was found not to reach the ceiling in all of the considered conditions, so these scenarios are not discussed in the experiments presented here. Also the tested velocities are all controlled to be less than the critical velocity, to have the flame extension beneath the ceiling both upstream and downstream. The maximum critical velocity, beyond which the upstream flame extension will disappear, is around 1.8 ~1.9 m/s for the highest heat release rate considered in these experiments. The longitudinal air flow speeds were measured by a hot-wire anemometer with accuracy of 0.01 m/s.

The flame extension length beneath the channel ceiling was recorded using a side-view CCD (Charge-Coupled Device) camera of sensor size 8.5 mm, with 3,000,000 pixels, at film speed of 25 frames per second. Quantification of the flame length was achieved using a visual scale with resolution of 0.1 m, attached to the channel side wall. A typical view of the flame extension phenomenon is shown in Fig. 2 (a). As similar to freely burning buoyant flames, the horizontally extending flame beneath the ceiling also exhibits considerable fluctuations. To account for these, time series flame videos have been decompressed into frames (60 s, 1500 frames). In order to get the flame extension

length, each image frame has been firstly converted to a gray scale image as shown in Fig. 2(b), and then to a binary image as shown in Fig. 2(c), based on the thresholds obtained objectively using the Otsu method [24-26]. Then, the binary images were averaged to get the flame intermittency contour as shown in Fig. 2(d), based on which the mean flame extension lengths were obtained at 50% intermittency. A typical image processing and comparison of flame lengths based on flame tip with the ones based on 50 % intermittency is shown in Fig. 2(e) as shown below.

(a) original image

(b) gray image

(c) binary image

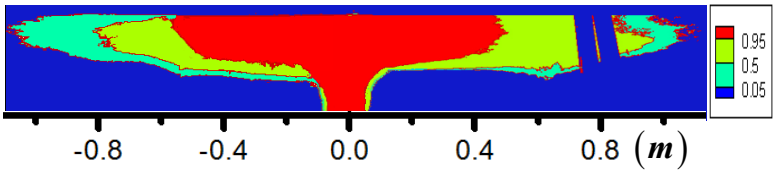

(d) mean flame contours

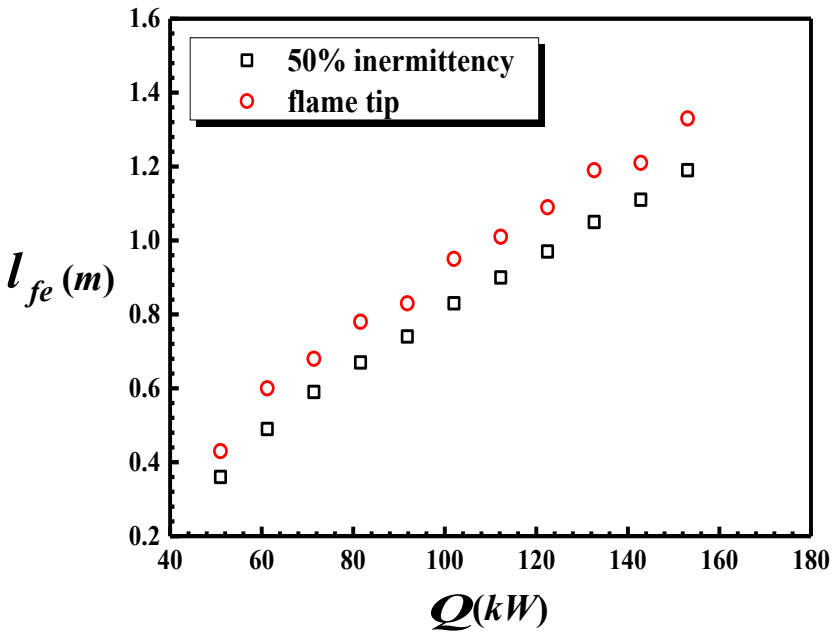

(e) Typical comparison of flame lengths based on flame tip with the ones of 50 % intermittency (channel width: 0.5 m; source size: 15 cm; source-ceiling height: 35 cm; no airflow).

Fig.2 Typical image processing of flame extension beneath the channel ceiling (channel width: 0.5 m; source size: 15 cm; source-ceiling height: 35 cm; HRR: 102.3 kW; no longitudinal air flow).

Total 469 experimental conditions involving various channel widths, fire source sizes, heat release rates, source-ceiling heights and longitudinal air flow speeds were considered. Each experimental condition lasted for 5 minutes at least, was repeated three times, and the average values were used for analysis and discussion. The test fire sizes as well as the longitudinal ventilation airflow speeds were carefully controlled at relatively small values to resolve the physics about the effect of longitudinal ventilation airflow on the un-burnt fuel distribution and air entrainment. All the experimental conditions and results are summarized in Table 1 (no longitudinal air flow) and Table 2 (with longitudinal air flow).

3. Results and discussion

3.1 Flame extension lengths beneath the ceiling

Figures 3 and 4 show the measured upstream and downstream flame extension lengths beneath the ceiling for various fire heat release rates, for different source-ceiling heights, with different longitudinal air flow speeds and burner sizes, in each of the two channel widths of 0.5 m and 1.5 m, respectively. It can be seen that:

(1) The flame extension length increases with increasing heat release rate, but decreases with increasing source-ceiling height or burner size (the decrease with increasing burner size is more remarkable as the source-ceiling height is larger or with a higher longitudinal air flow speed) for all conditions. The flame extension length is larger when the channel width is narrower.

(2) The flame extension lengths with a longitudinal air flow are measurably different from those with no air flow. The length is considerably larger with no longitudinal air flow (the flame extension lengths for upstream and downstream are nearly same with a difference quantified to be less than 5%, and an average value is presented here) than that even with a low longitudinal air flow (i.e. 0.3 m/s, 0.6 m/s). This could be due to flame tilt leading to a longer section of flame before the point of impingement, resulting in less un-burnt fuel remaining after impingement. This then requires a smaller amount of air entrainment to consume the un-burnt fuel, which leads to a shorter flame extension length.

(3) With a longitudinal air flow, the flame extension length is shorter upstream than downstream. This is due to the asymmetrical (unburnt) fuel distribution at the two sides of the source. There is comparatively less unburnt fuel on the upstream side due to the opposed flow condition, meanwhile comparatively more fuel on the downstream side due to the concurrent flow condition.

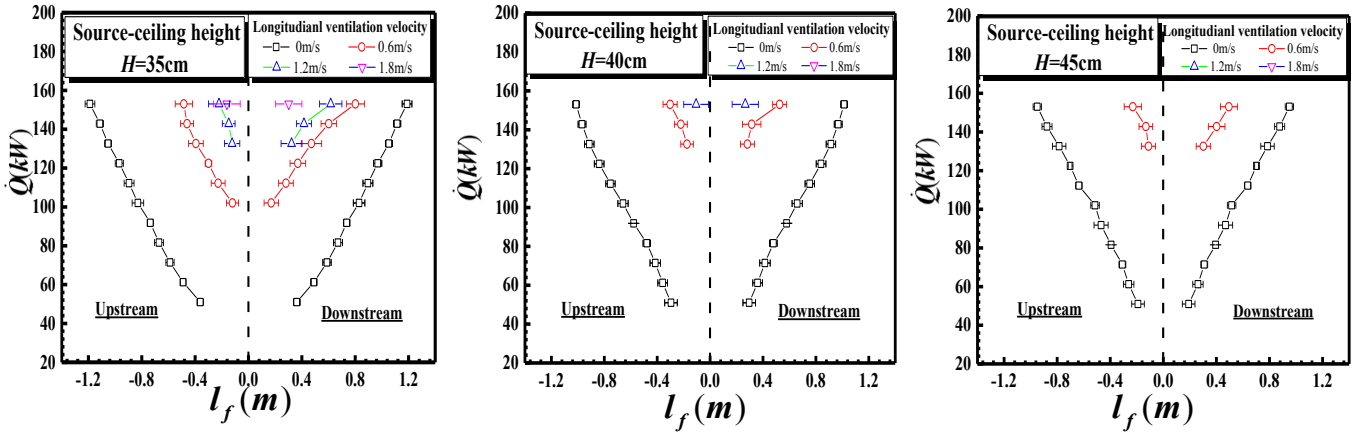

(a) burner size of 15 cm

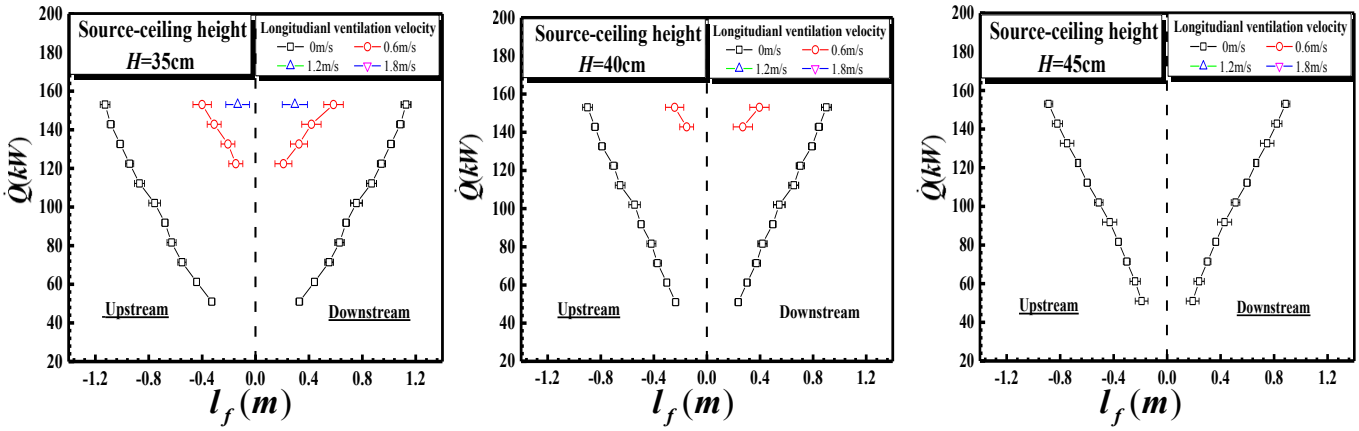

(b) burner size of 20 cm

Fig. 3 Measured upstream and downstream flame extension lengths beneath ceiling (channel width-0.5 m)

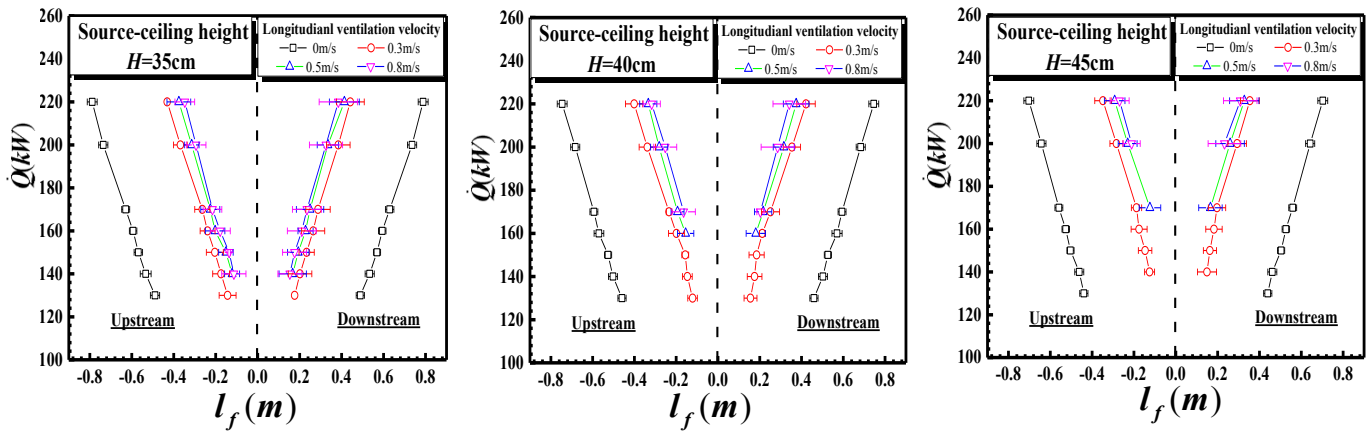

(a) burner size of 25 cm

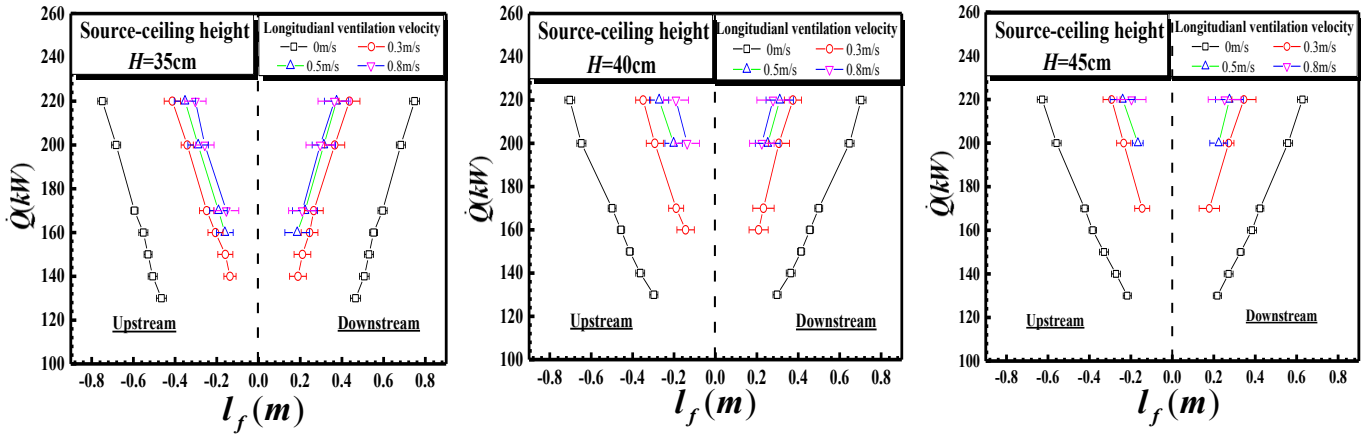

(b) burner size of 30 cm

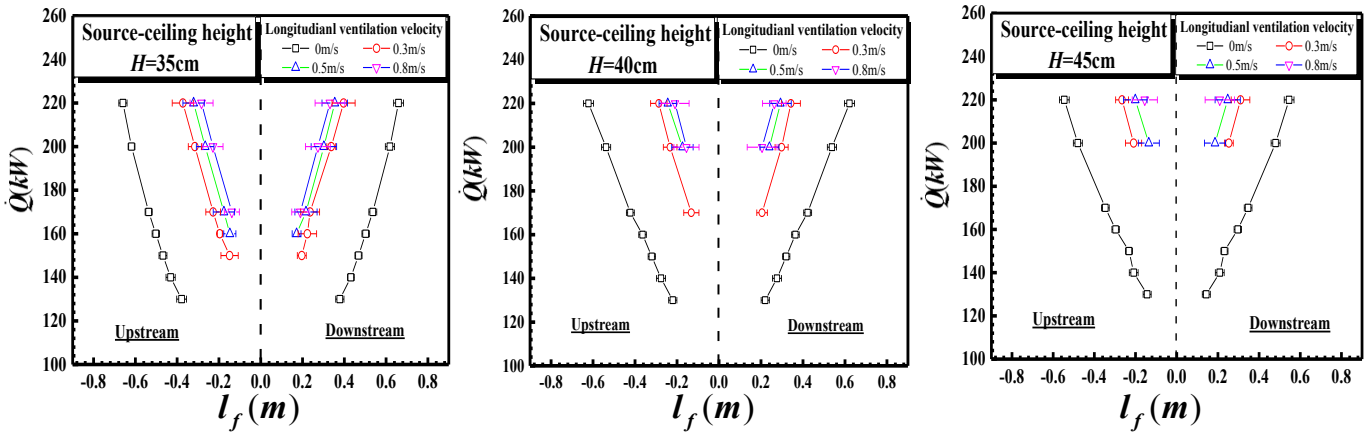

(c) burner size of 35 cm

Fig. 4 Measured upstream and downstream flame extension lengths beneath ceiling (channel width-1.5 m)

Figures 5 and 6 present the total flame extension lengths (upstream plus downstream) beneath the ceiling for various fire heat release rates, source-ceiling heights, longitudinal air flow speeds and burner sizes, for the two channel widths of 0.5 m and 1.5 m, respectively. The total flame extension length also increases with increasing heat release rate, but decreases with increasing the source-ceiling height or longitudinal air flow speed. The total flame extension length is larger in the narrower channel.

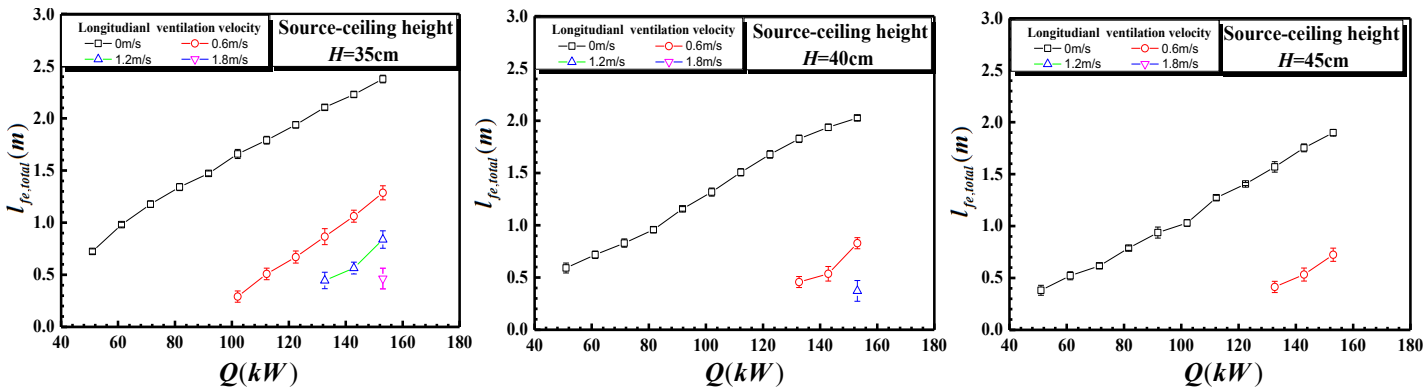

(a) burner size of 15 cm

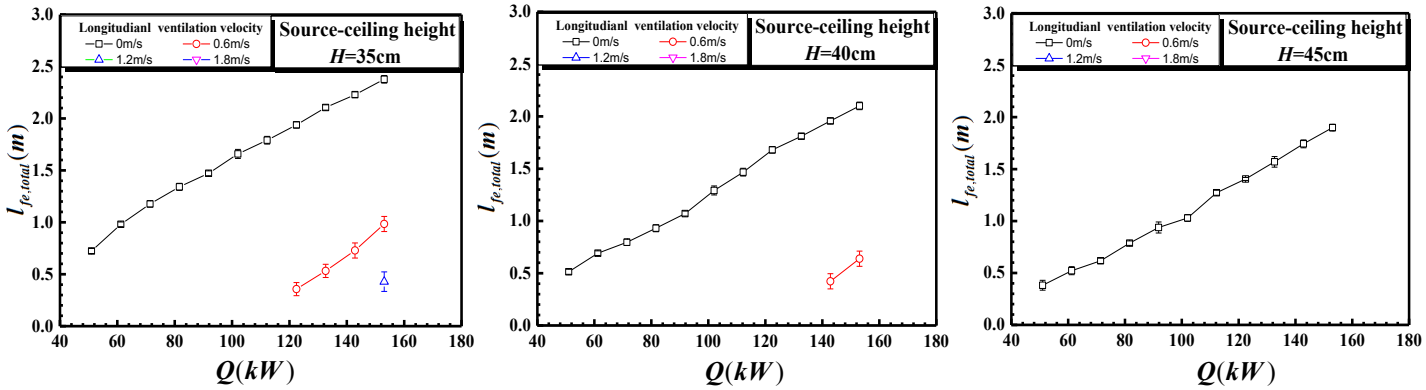

(b) burner size of 20 cm

Fig. 5 Measured total flame extension lengths beneath ceiling

(channel width-0.5 m)

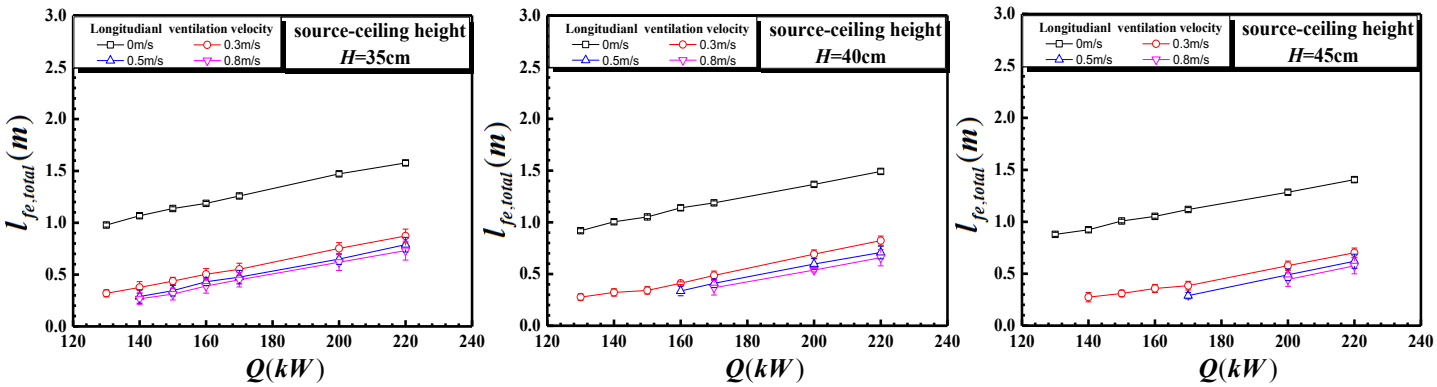

(a) burner size of 25 cm

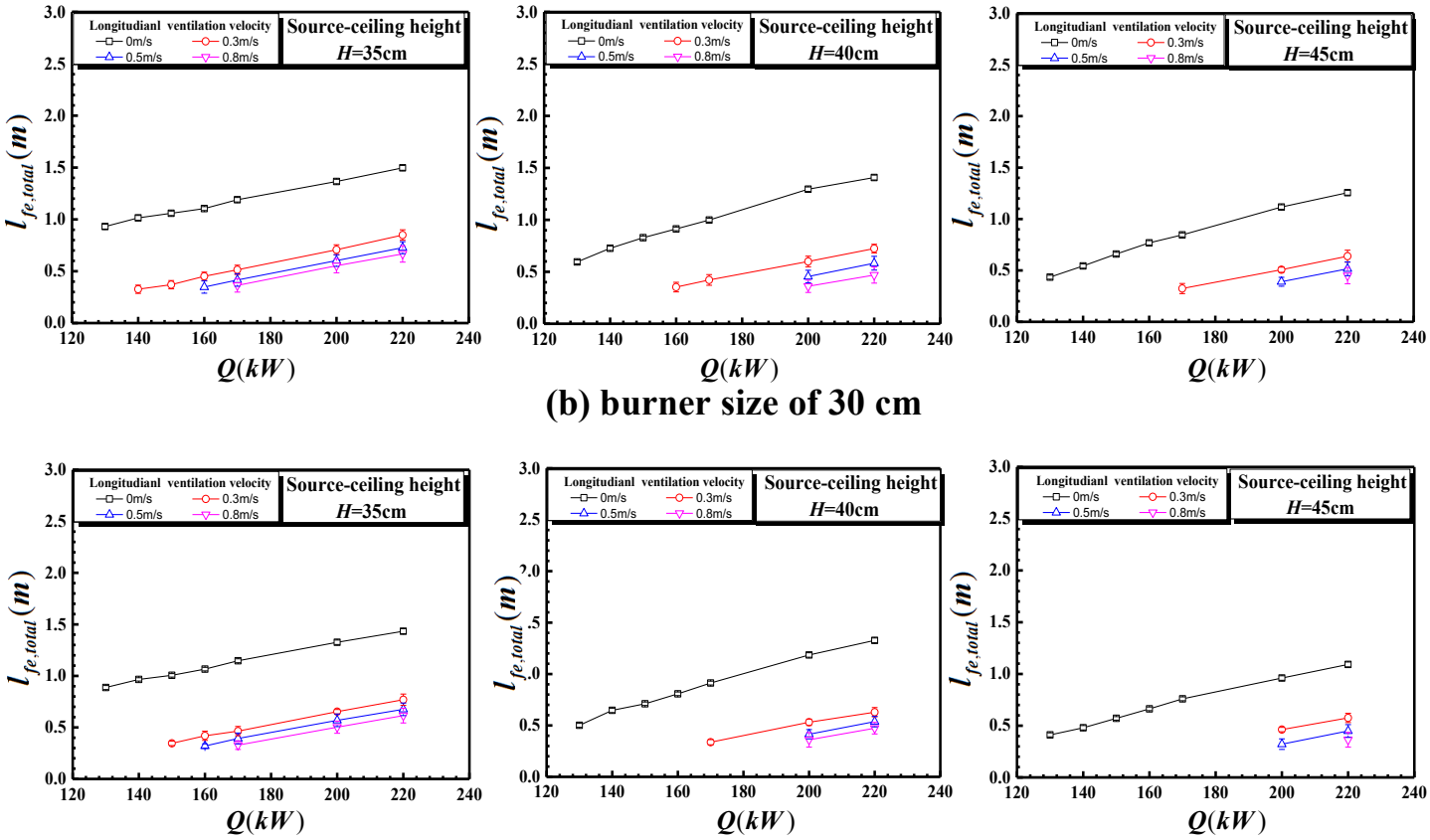

(b) burner size of 30 cm

(c) burner size of 35 cm

Fig. 6 Measured total flame extension lengths beneath ceiling (channel width-1.5 m)

Physically, the flame extension length beneath the channel ceiling should be related to the unburnt portion of the fuel after impingement and to the air entrainment into the impinged ceiling flow, which consumes the unburnt fuel traveling beneath the ceiling. Following these observations, the measured flame extension lengths have been correlated non-dimensionally in relation to the total fire heat release rate (Q), source-ceiling height (H), channel ceiling width (W), as well as longitudinal air flow speed (u_a), as discussed in the following sections. Since the flame extension with no longitudinal air flow is observed to be clearly different from that with a longitudinal air flow as shown in Figs. 3-6 (this might due to complicated nature of the interaction of the buoyancy-induced flow with longitudinal air flow (even with low speed) once it is involved), correlations are proposed separately for the results with no longitudinal air flow (section 3.2) and those with longitudinal air flows (section 3.3), respectively.

3.2 Correlation of flame extension length with no longitudinal air flow

In order to consume the unburnt fuel after impingement, the heat of combustion of the air entrained into the ceiling flow should be proportional to the heat of combustion of the unburnt fuel:

$$\rho_\infty \Delta H_\infty u_e l_{fe,0} W \sim \left[\frac{H_f - H}{H_f}\right] \rho_{fuel} \Delta H_{fuel} V_{fuel} \sim \left[\frac{H_f - H}{H_f}\right] Q_{fuel} \tag{6}$$

In Eq. (6), the Right Hand Side (RHS) of the formula is the portion of the heat released of un-burnt fuel after impingement on the ceiling (assuming the heat is released uniformly along the length of the flame, i.e. as similarly treated by You and Faeth [1] as indicated in Eq. 1), where Q_{fuel} is the total HRR, H_f is the free flame height with no airflow, whose values were estimated by the well-known formula proposed by Heskestad [27] which is widely used in practice:

$$H_f = -1.02D + 0.235Q^{2/5} \tag{7}$$

and the estimated values of H_f for the present experiments were summarized in Table 1, H is source-ceiling height, and $\left[\frac{H_f - H}{H_f}\right]$ is the ratio of un-burnt fuel; the Left Hand Side (LHS) of the formula is the heat released counted by the air entrained into the ceiling flow, where ΔH_∞ is the heat of combustion for air, that is, the heat released per kg of air consumed, with a value of 3013 kJ/kg. W is the channel width, $l_{fe,0}$ is flame extension length along the channel ceiling with no air flow, V_{fuel} is the volumetric fuel flow rate, and u_e is the characteristic air entrainment velocity into the ceiling flow after impingement. u_e is assumed to be proportional to the buoyancy-accelerated upward velocity of the flame immediately before the impingement, which is:

$$u_e \sim \sqrt{2\frac{\Delta\rho_f}{\rho_\infty} gH} \tag{8}$$

where $\Delta\rho_f$ is the density difference between flame(ρ_f) and ambient air(ρ_∞), ρ_∞ is the ambient air density, ρ_f is the density of the flame (0.32 kg/m^3 ; assuming a flame temperature of 1100 K) and g is

gravitational acceleration (9.8 m/s^2). Substituting Eq. (8) into Eq. (6), it gives:

$$\rho_\infty \Delta H_\infty l_{fe,0} W \sqrt{2\frac{\Delta\rho_f}{\rho_\infty} gH} \sim \left[\frac{H_f - H}{H_f}\right] Q_{fuel} \tag{9}$$

Thus, the flame extension length beneath channeled ceiling with no air flow ($l_{fe,0}$) can be expressed as:

$$l_{fe,0} \sim \frac{\left[\frac{H_f - H}{H_f}\right] Q_{fuel}}{\rho_\infty \Delta H_\infty W \sqrt{2\frac{\Delta\rho_f}{\rho_\infty} gH}} \tag{10a}$$

or non-dimensionally:

$$\frac{l_{fe,0}}{D} \sim \left[\frac{\left(\frac{H_f - H}{H_f}\right)}{\sqrt{2\frac{\Delta\rho_f}{\rho_\infty}}}\right] Q^{**}_{fuel} \tag{10b}$$

Here, the new non-dimensional heat release rate is defined as:

$$Q^{**}_{fuel} = \frac{Q_{fuel}}{\rho_\infty \Delta H_\infty \sqrt{gH} WD} \tag{11}$$

Figure 7 shows that the measured flame extension lengths with no air flow fit well to the proposed model (Eq. 11), using a proportionality constant of 10.20, which gives:

$$\frac{l_{fe,0}}{D} = 10.20 \left[\frac{\left(\frac{H_f - H}{H_f}\right)}{\sqrt{2\frac{\Delta\rho_f}{\rho_\infty}}}\right] Q^{**}_{fuel} \tag{12}$$

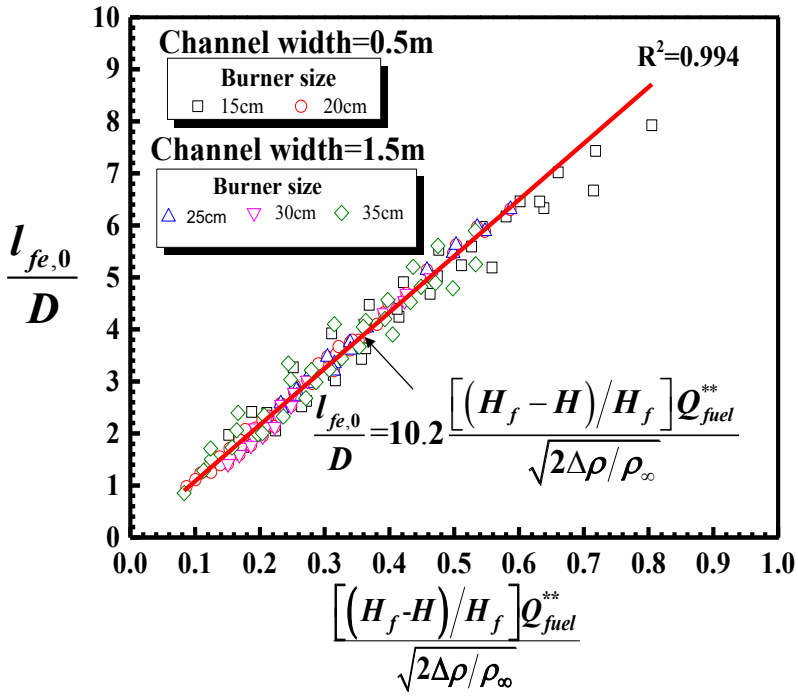

Fig. 7 Non-dimensional correlation of flame extension length beneath channel ceiling with no longitudinal air flow

The data obtained and the correlation was found be much less than those reported in Hinkley's work [9, 10]. However, it should be noted that Hinkley's experimental condition is fundamentally different:

(1) Hinkley's experiments were carried out in a model representing a corridor with a fire source at the (closed) rear end of the corridor. It is expected that this configuration would result in a stronger confinement of air entrainment, that is, the rate of entrainment of air will be much less than if the fire source is positioned in the middle of the ceiling (as in the present work), which would result in more un-burnt fuel remaining after impingement and then require more air entrainment to consume the un-burnt fuel, leading to a relatively longer flame extension length in Hinkley's work.

(2) The extension length of horizontal flame was measured to the flame tip by using visual observation in Hinkley's work rather than the mean flame extension lengths in the present work. That results in relatively longer estimated flame extension lengths in Hinkley's work than those in the present work.

3.3 Correlation of flame extension lengths (upstream, downstream and the total length) with a longitudinal air flow

When a longitudinal air flow less than the critical velocity is imposed, the flame extension is longer downstream than upstream. This is physically due to the smaller portion of unburnt fuel present upstream, compared with downstream, which is attributed to the different ceiling flow directions relative to the air flow. There is currently no theory about the distribution of the flame extension length upstream and downstream under longitudinal ventilation flow conditions in a tunnel. In order to characterize the distribution of unburnt fuel for the upstream and downstream sides, due to the longitudinal air flow imposed, we introduce the assumption that the difference between the upstream and downstream flame extension length can be empirically represented as a function of the magnitude of the longitudinal air flow speed (u_a) relative to the effective impinged flow speed, which could be assumed to be proportional to the buoyancy-accelerated uprising velocity right before impingement ($\sqrt{2\frac{\Delta\rho_f}{\rho_\infty}gH}$, whose values are calculated to range from 2.24 to 2.55 m/s (given in Table 2), which are comparable to u_a.). Hence, the distribution of un-burnt fuel is proposed to be $\left[\frac{\alpha\sqrt{2\frac{\Delta\rho_f}{\rho_\infty}gH}-u_a}{2\alpha\sqrt{2\frac{\Delta\rho_f}{\rho_\infty}gH}}\right]Q_{fuel}$ for the upstream, and to be $\left[\frac{\alpha\sqrt{2\frac{\Delta\rho_f}{\rho_\infty}gH}+u_a}{2\alpha\sqrt{2\frac{\Delta\rho_f}{\rho_\infty}gH}}\right]Q_{fuel}$ for the downstream respectively; or namely $\alpha\sqrt{2\frac{\Delta\rho_f}{\rho_\infty}gH}$ can be deemed as the effective impinged flow speed to compare with the longitudinal air flow speed (u_a). Note that when the longitudinal air flow speed is high enough, the upstream flame extension will be eliminated by the air flow; this scenario is not considered in the current study. In a manner similar to Eq. (6), considering the distribution of unburnt fuel for the upstream and

downstream and the consumption of the unburnt fuel by the entrained air after impingement, the following expressions for the upstream side and the downstream side can be obtained, respectively:

for the upstream:

$$\rho_\infty \Delta H_\infty u_e l_{fe,upstream} W \sim \left(\frac{H_f - H/\cos\theta}{H_f} \right) \left[\frac{\alpha \sqrt{2 \frac{\Delta\rho_f}{\rho_\infty} gH} - u_a}{2\alpha \sqrt{2 \frac{\Delta\rho_f}{\rho_\infty} gH}} \right] Q_{fuel} \tag{13a}$$

for the downstream:

$$\rho_\infty \Delta H_\infty u_e l_{fe,downstream} W \sim \left(\frac{H_f - H/\cos\theta}{H_f} \right) \left[\frac{\alpha \sqrt{2 \frac{\Delta\rho_f}{\rho_\infty} gH} + u_a}{2\alpha \sqrt{2 \frac{\Delta\rho_f}{\rho_\infty} gH}} \right] Q_{fuel} \tag{13b}$$

where $l_{fe,upstream}$ and $l_{fe,downstream}$ are the flame extension lengths beneath the channeled ceiling for upstream and downstream with an imposed air flow. In this study we used a gaseous fuel and the longitudinal ventilation airflow velocity is controlled at relatively low level (less than the critical velocity to have both upstream and downstream flame extension length). It is assumed that the total flame length is un-affected by the longitudinal ventilation airflow in these designed scenarios. Thus, $\left(\frac{H_f - H/\cos\theta}{H_f} \right)$ was introduced to represent the un-burnt fuel beneath the ceiling after impingement under longitudinal ventilation airflow conditions, in which the flame tilt angle (θ) can be calculated by the formula proposed in [28]:

$$\theta = \arctan\left[9.1 \left(\frac{\rho_\infty c_p \Delta T_f u_a^{\,5}}{Q_{fuel}} \cdot \left(\frac{T_\infty}{g \Delta T_f} \right)^2 \right)^{1/5} \right] \tag{14}$$

where ΔT_f is taken as a constant (800 K).

Substituting Eq. (8) into Eq. (13a) and Eq. (13b), the upstream and downstream flame extension

lengths can be expressed non-dimensionally as (similar to Eq. 10b):

for the upstream:

$$\frac{l_{fe,upstream}}{D} \sim \left(\frac{H_f - H/\cos\theta}{H_f} \right) \left[\frac{\alpha\sqrt{2\frac{\Delta\rho_f}{\rho_\infty} gH} - u_a}{2\alpha\sqrt{2\frac{\Delta\rho_f}{\rho_\infty} gH}} \right] Q^{**}_{fuel} \tag{15a}$$

for the downstream:

$$\frac{l_{fe,downstream}}{D} \sim \left(\frac{H_f - H/\cos\theta}{H_f} \right) \left[\frac{\alpha\sqrt{2\frac{\Delta\rho_f}{\rho_\infty} gH} + u_a}{2\alpha\sqrt{2\frac{\Delta\rho_f}{\rho_\infty} gH}} \right] Q^{**}_{fuel} \tag{15b}$$

It is noted that the following requirements are needed:

for the upstream,

$$\frac{\alpha\sqrt{2\frac{\Delta\rho_f}{\rho_\infty} gH} - u_a}{2\alpha\sqrt{2\frac{\Delta\rho_f}{\rho_\infty} gH}} \geq 0 \tag{16a}$$

while for the downstream,

$$\frac{\alpha\sqrt{2\frac{\Delta\rho_f}{\rho_\infty} gH} + u_a}{2\alpha\sqrt{2\frac{\Delta\rho_f}{\rho_\infty} gH}} \leq 1 \tag{16b}$$

The above requires that

$$\alpha \geq \frac{u_a}{\sqrt{2\frac{\Delta\rho_f}{\rho_\infty} gH}} \tag{17}$$

According to the experimental conditions in Table 2, the value of u_a is 0.6, 1.2, 1.8 m/s; while the value of $\sqrt{2\frac{\Delta\rho_f}{\rho_\infty} gH}$ is 2.24, 2.4, 2.55. This gives that their maximum ratio of $\frac{u_a}{\sqrt{2\frac{\Delta\rho_f}{\rho_\infty} gH}}$

considered in the present experiments is

$$\left(\frac{u_a}{\sqrt{2\frac{\Delta\rho_f}{\rho_\infty}gH}}\right)_{\max} = \frac{1.8}{2.24} \approx 0.80 \tag{18}$$

So, the value of α should have

$$\alpha \geq 0.8 \tag{19}$$

There is still no work reported yet to show what value should be taken for this coefficient, α. Hence, we have considered three different values of α empirically as 0.8, 0.9 and 1.0 to find which value could have a best fit of the data. The fitting results of the experimental data with different values of α as 0.8, 0.9 and 1.0 for the upstream and downstream is given in Figs. 8 and 9, respectively.

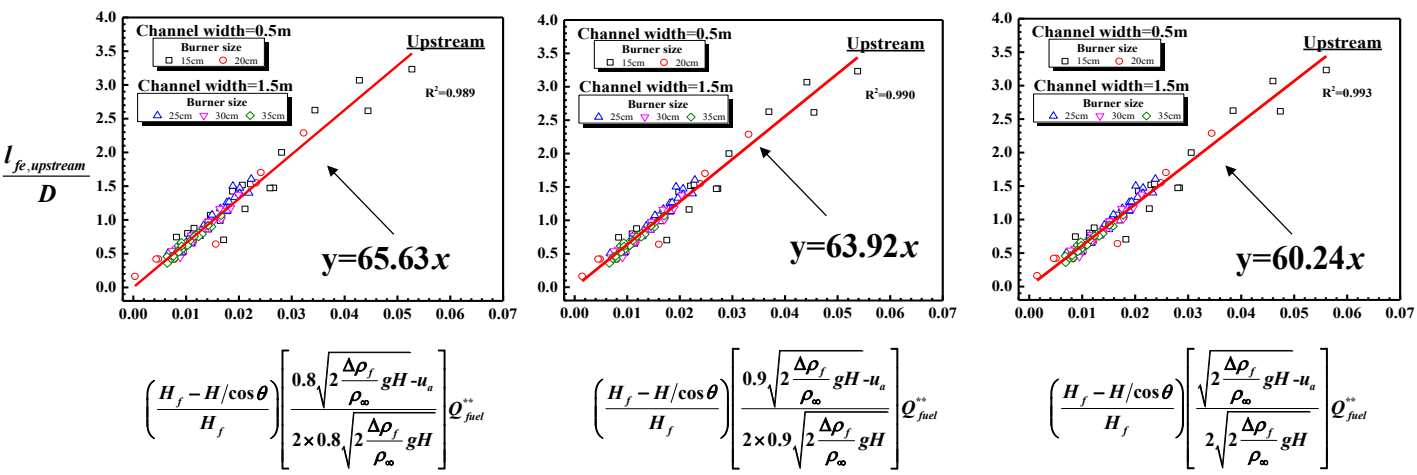

(a) α=0.8 **(b) α=0.9** **(c) α=1.0**

Fig. 8 Non-dimensional correlation of upstream flame extension length beneath channel ceiling with longitudinal air flow with α = 0.8, 0.9, 1.0 respectively, showing a relatively best fit is reached with α=1.0 for the present experiments.

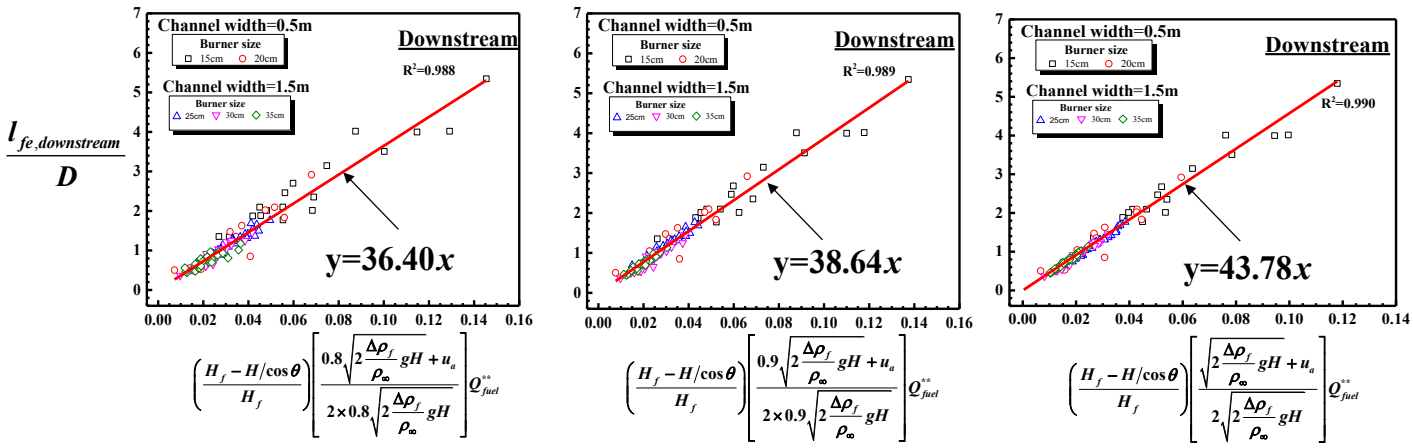

(a) α=0.8 (b) α=0.9 (c) α=1.0

Fig. 9 Non-dimensional correlation of downstream flame extension length beneath channel ceiling with longitudinal air flow with α = 0.8, 0.9, 1.0 respectively, showing a relatively best fit is reached with α=1.0 for the present experiments.

Results show that the correlation coefficient value (R^2) do not change considerably with these three different values of α. However, the data showed to be best fitted with the value of α as 1.0, which is selected as the value to be used for the present experiments. Then, the following formulae (Eqs. 20a or 20b) are suggested for the upstream and downstream flame extension lengths, respectively:

$$\frac{l_{fe,upstream}}{D} = 60.24\left(\frac{H_f - H/\cos\theta}{H_f}\right)\left[\frac{\sqrt{2\frac{\Delta\rho_f}{\rho_\infty}gH} - u_a}{2\sqrt{2\frac{\Delta\rho_f}{\rho_\infty}gH}}\right]Q^{**}_{fuel} \qquad (0.199 \le Q^{**}_{fuel} \le 0.427, 0.3 \le u_a \le 1.8) \qquad (20a)$$

$$\frac{l_{fe,downstream}}{D} = 43.78\left(\frac{H_f - H/\cos\theta}{H_f}\right)\left[\frac{\sqrt{2\frac{\Delta\rho_f}{\rho_\infty}gH} + u_a}{2\sqrt{2\frac{\Delta\rho_f}{\rho_\infty}gH}}\right]Q^{**}_{fuel} \qquad (0.199 \le Q^{**}_{fuel} \le 0.427, 0.3 \le u_a \le 1.8) \qquad (20b)$$

However, it should be noted that the selection of α as 1.0 is currently just limited for the present experiments. Broader range of experiments in the future might suggest more suitable value of this coefficient in general. This needs to be further validated in the future investigation.

Now, based on Eqs. (20a) and (20b) describing the flame extension lengths of upstream and downstream, respectively, the total flame extension length ($l_{fe,total}$) can be obtained by:

$$\frac{l_{fe,total}}{D}=\frac{l_{fe,upstream}+l_{fe,downstream}}{D}=\left[\frac{104.02\sqrt{2\frac{\Delta\rho_f}{\rho_\infty}gH}-16.46u_a}{\sqrt{2\frac{\Delta\rho_f}{\rho_\infty}gH}}\right]\left(\frac{H_f-H/\cos\theta}{H_f}\right)Q^{**}_{fuel} \tag{21a}$$

By noting that $104.02\sqrt{2\frac{\Delta\rho_f}{\rho_\infty}gH}>>16.46u_a$, the above formula can be further simplified as,

$$\frac{l_{fe,total}}{D}=104.02\left(\frac{H_f-H/\cos\theta}{H_f}\right)Q^{**}_{fuel} \qquad (0.199\le Q^{**}_{fuel}\le 0.427, 0.3\le u_a\le 1.8) \tag{21b}$$

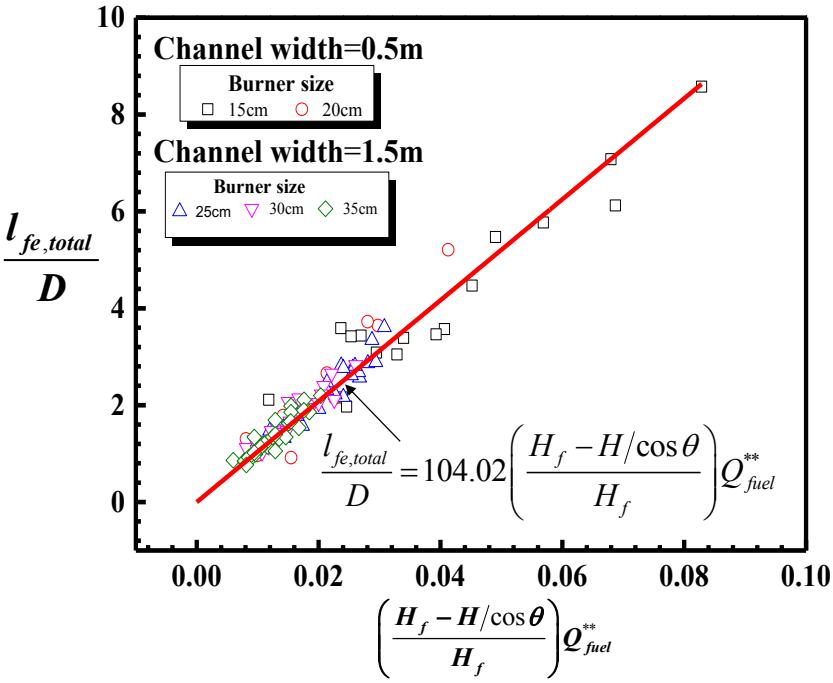

Fig. 10 Comparison of predicted total flame extension length beneath channel ceiling with longitudinal air flow (Eq. 21b) with measured values

Figure 10 shows that the relationship between the measured total flame extension lengths and the longitudinal air flow speeds are well represented by the proposed formula (Eq. 21b). It should be noted that the above correlations are only applicable with an imposed longitudinal ventilation velocity. This is similar to the condition about the previous correlation on flame length in crosswind proposed by

Thomas [29], Rew and Deaves [30] for which the flame length would appear to be infinite if the wind speed was zero.

4. Conclusions

This paper investigates flame extension lengths (upstream, downstream, as well as their total length) beneath a confined ceiling for a fire in a channel, with longitudinal air flows, for various heat release rates, burner sizes, channel widths and source-ceiling heights. The major findings include:

(1) The flame extension lengths (upstream, downstream, as well as their total length) beneath a channel ceiling increase with heat release rate, and decrease with source-ceiling height, channel width, burner size, or longitudinal air flow speed (see Figs. 3-6). With a longitudinal air flow but less than the critical velocity, the flame extension length is longer downstream than upstream (see Figs. 3 and 4).

(2) Non-dimensional correlations have been proposed for the flame extension lengths (both upstream and downstream after impingement) based on physically the unburnt fuel distribution (upstream and downstream), as well as considering air entrainment of the impinged ceiling flow to further consume the unburnt fuel beneath the ceiling. The proposed formulae have been shown to correlate well with the data for the no air flow scenarios (Eq. 12; Fig. 7) and those with various longitudinal air flow speeds (Eq. 20; Figs. 8 and 9).

(3) A formula to estimate the total flame extension lengths with longitudinal air flows has been developed (Eq. 21b), based on the correlations of flame extension length for both upstream and downstream. The proposed formula has been shown to represent the measured data well (Fig. 10).

In the present work, the test fire sizes as well as the longitudinal ventilation airflow speed are carefully controlled at relatively small values to adequately resolve the physics about the effect of longitudinal ventilation airflow on the un-burnt fuel distribution and air entrainment, hence the flame

extension length beneath the ceiling both upstream and downstream. Additional larger scale tests, carried out in the future, will be helpful to validate the above correlations.

Acknowledgement

This work was supported jointly by the National Key R&D Program of China under Grant No. 2016YFC0800603, National Natural Science Foundation of China (NSFC) under Grant No. 51704244, Key Project of NSFC under Grant No. 51636008, the Newton Advanced Fellowship (NSFC: 51561130158; RS: NA140102), the Key Research Program of Frontier Sciences, Chinese Academy of Science (CAS) under Grant No.QYZDB-SSW-JSC029, NSFC-STINT joint project (USTC-Lund University), the Fok Ying-Tong Education Foundation under Grant No. 151056, the Fundamental Research Funds for the Central Universities under Grant No. WK2320000035 and the Opening Fund of State Key Laboratory of Fire Science (Grant No. HZ2017-KF11).

References

[1] H.Z. You, G.M. Faeth, Ceiling heat transfer during fire plume and fire impingement. Fire Mater. 3 (1979) 140-147.

[2] V. Babrauskas, Flame lengths under ceilings. Fire Mater. 4 (3) (1980) 119-126.

[3] D. Gross, Measurement of flame lengths under ceilings, Fire Saf. J. 15 (1989) 31-44.

[4] Y. Hasemi, S. Yokobayashi, T. Wakamatsu, A. Ptchelintsev, Flame heat transfer and concurrent flame spread in a ceiling fire, ASIAFLAM (1995) 351-366.

[5] B.Y. Lattimer, Heat fluxes and flame lengths from fires under ceilings, Fire Technol. 49 (2013) 269-291.

[6] H.W. Ding, J.G. Quintiere, An integral model for turbulent flame radial lengths under a ceiling, Fire Saf. J.. 52 (2012) 25-33.

[7] X.C. Zhang, L.H. Hu, W. Zhu, X.L. Zhang, L.Z. Yang, Flame extension length and temperature profile in thermal impinging flow of buoyant round jet upon a horizontal plate, Appl. Therm. Eng. 73 (2014) 15-22.

[8] X.C. Zhang, H.W. Tao, W.B. Xu, X.Z. Liu, X.L. Zhang, L.H. Hu, Flame extension lengths beneath an inclined ceiling induced by rectangular-source fires, Combust. Flame, 176 (2017) 349-357.

[9] P.L. Hinkley, H.G.H. Wraight, C.R. Theobald, The contribution of flames under ceilings to fire spread in compartments, Fire Saf. J. 7 (1984) 227-242.

[10] P.L. Hinkley, H.G.H. Wraight, C.R. Theobald, The contribution of flames under ceilings to fire spread in compartments, Fire Research Note No. 712, Fire Research Stations, Borehamwood, Herts, UK, 1968.

[11] A. Kashef, Z. Yuan, B. Lei. Ceiling temperature distribution and smoke diffusion in tunnel fires with natural ventilation. Fire Saf. J. 62 (2013) 249-255.

[12] Y. P. Lee, K. C. Tsai. Effect of vehicular blockage on critical ventilation velocity and tunnel fire behavior in longitudinally ventilated tunnels, Fire Saf. J. 53 (2012) 35-42.

[13] W. Ulises Rojas Alva, Grunde Jomaas, Anne S. Dederichs, The influence of vehicular obstacles on longitudinal ventilation control in tunnel fires, Fire Saf. J. 87 (2017) 25-36.

[14] X.Y. Wang, M.J. Spearpoint, C.M. Fleischmann, Investigation of the effect of tunnel ventilation on crib fires through small-scale experiments, Fire Saf. J. 88 (2017) 45-55.

[15] F. Tanaka, S. Majima, M. Kato, N. Kawabata, Performance validation of a hybrid ventilation strategy comprising longitudinal and point ventilation by a fire experiment using a model-scale tunnel, Fire Saf. J. 71 (2015) 287-298.

[16] W.K. Chow, Y. Gao, J.H. Zhao, J.F. Dang, C.L. Chow, L. Miao, Smoke movement in tilted tunnel fires with longitudinal ventilation, Fire Saf. J. 75 (2015) 14-22.

[17] Y.Z. Li, H. Ingason. Fire-induced ceiling jet characteristics in tunnels under different ventilation conditions, 2015. SP Report 2015:23.

[18] H. Ingason, Y.Z. Li, Model scale tunnel fire tests with longitudinal ventilation, Fire Saf. J. 45 (2010) 371-384.

[19] Y.Z. Li, Study of fire characteristics and smoke control in super long tunnels with rescue station (Ph.D. thesis), Southwest Jiaotong University, 2010.

[20] H. Ingason, Y.Z. Li, A. Lönnermark, Tunnel fire dynamics, 2014.

[21] Fires in Transport Tunnels: Report on Full-Scale Tests, 1995, edited by Stahlanwendung e.V., EUREKA-Project EU499, FIRETUN, Dusseldorf, Germany, 1995.

[22] Memorial Tunnel Fire Ventilation Test Program - Test Report, 1995, Massachusetts Highway Department and Federal Highway Administration.

[23] A. Lönnermark, H. Ingason, Fire spread and flame length in large-scale tunnel fires. Fire Technol. 2006. 42(4): p. 283-302.

[24] L.F. Chen, L.H. Hu, W. Tang, L. Yi, Studies on buoyancy driven two-directional smoke flow layering length with combination of point extraction and longitudinal ventilation in tunnel fires, Fire Saf. J. 59 (2013) 94-101.

[25] L.H. Hu, K. H. Lu, M.A. Delichatsios, L.H. He, F. Tang, An experimental investigation and statistical characterization of intermittent flame ejecting behavior of enclosure fires with an opening Combust. Flame 159 (2012) 1178-1184.

[26] N. Otsu, A Threshold Selection Method from Gray-Level Histograms, IEEE Trans, Syst. Man. Cyb. 9 (1979) 62-66.

[27] Heskestad G., Fire Plumes, Flame Height, and Air Entrainment. In: Hurley M.J. et al. (eds) SFPE Handbook of Fire Protection Engineering. Springer, New York, NY(2016).

[28] L.H. Hu, S. Liu, J.L. de Ris, L. Wu, A new mathematical quantification of wind-blown flame tilt angle of hydrocarbon pool fires with a new global correlation model, Fuel 106 (2013) 730-736.

[29] P .Thomas, The movement of buoyant fluid against a stream and the venting of underground fires. Fire Research Station, F.R. Note No.351/1958, Boreham Wood, 1958.

[30] C. Rew, D. Deaves, Fire spread and flame length in ventilated tunnels-a model used in Channel tunnel assessments, in: Proceedings of the International Conference on Tunnel Fires and Escape from Tunnels, Lyon, France, 5-7 May 1999, pp.397-406.

Table 1 Summary of experimental conditions and results with no longitudinal air flow

Test No.	W (m)	D (m)	H (m)	Q (kW) Q^{**} (Eq. 10) H_f (m)* $l_{fe,0}$ (m) $l_{fe,total}$ (m)										
				51.0	**61.2**	**71.4**	**81.6**	**91.8**	**102.0**	**112.2**	**122.4**	**132.6**	**142.8**	**153.0**
				0.111	0.133	0.155	0.177	0.200	0.222	0.244	0.266	0.288	0.310	0.332
1-11	0.5	0.15	0.35	1.42	1.53	1.63	1.73	1.81	1.89	1.97	2.04	2.11	2.17	2.23
				0.36	0.49	0.59	0.67	0.74	0.83	0.90	0.97	1.05	1.11	1.19
				0.72	0.98	1.18	1.34	1.47	1.66	1.80	1.94	2.10	2.22	2.38
				51.0	**61.2**	**71.4**	**81.6**	**91.8**	**102.0**	**112.2**	**122.4**	**132.6**	**142.8**	**153.0**
				0.127	0.152	0.177	0.203	0.228	0.253	0.279	0.304	0.329	0.355	0.380
12-22	0.5	0.15	0.40	1.42	1.53	1.63	1.73	1.81	1.89	1.97	2.04	2.11	2.17	2.23
				0.29	0.36	0.41	0.48	0.58	0.66	0.75	0.84	0.91	0.97	1.01
				0.54	0.72	0.82	0.96	1.16	1.22	1.30	1.68	1.82	1.94	2.02
				51.0	**61.2**	**71.4**	**81.6**	**91.8**	**102.0**	**112.2**	**122.4**	**132.6**	**142.8**	**153.0**
				0.142	0.171	0.200	0.228	0.256	0.285	0.313	0.342	0.370	0.400	0.427
23-33	0.5	0.15	0.45	1.42	1.53	1.63	1.73	1.81	1.89	1.97	2.04	2.11	2.17	2.23
				0.19	0.26	0.31	0.39	0.47	0.51	0.64	0.70	0.78	0.88	0.95
				0.38	0.52	0.62	0.78	0.94	1.02	1.28	1.4	1.56	1.76	1.90
				51.0	**61.2**	**71.4**	**81.6**	**91.8**	**102.0**	**112.2**	**122.4**	**132.6**	**142.8**	**153.0**
				0.083	0.100	0.116	0.133	0.149	0.166	0.182	0.199	0.216	0.232	0.249
34-44	0.5	0.20	0.35	1.41	1.52	1.62	1.71	1.80	1.88	1.95	2.02	2.10	2.16	2.22
				0.32	0.44	0.55	0.63	0.68	0.75	0.87	0.94	1.01	1.08	1.12
				0.64	0.88	1.10	1.26	1.36	1.5.0	1.74	1.88	2.02	2.16	2.24
				51.0	**61.2**	**71.4**	**81.6**	**91.8**	**102.0**	**112.2**	**122.4**	**132.6**	**142.8**	**153.0**
				0.077	0.093	0.109	0.124	0.140	0.155	0.171	0.186	0.202	0.218	0.233
45-55	0.5	0.20	0.40	1.41	1.52	1.62	1.71	1.80	1.88	1.95	2.02	2.10	2.16	2.22
				0.23	0.30	0.37	0.42	0.50	0.55	0.65	0.70	0.79	0.84	0.90
				0.46	0.60	0.74	0.84	1.00	1.10	1.30	1.40	1.58	1.68	1.8
				51.0	**61.2**	**71.4**	**81.6**	**91.8**	**102.0**	**112.2**	**122.4**	**132.6**	**142.8**	**153.0**
				0.073	0.088	0.103	0.117	0.132	0.146	0.161	0.176	0.191	0.205	0.220
56-66	0.5	0.20	0.45	1.41	1.52	1.62	1.71	1.80	1.88	1.95	2.02	2.10	2.16	2.22
				0.17	0.24	0.30	0.36	0.43	0.51	0.60	0.66	0.75	0.82	0.89
				0.34	0.48	0.60	0.72	0.86	1.02	1.20	1.32	1.50	1.64	1.78
				130	**140**	**150**	**160**	**170**	**200**	**220**				
				0.053	0.057	0.061	0.065	0.069	0.081	0.089				
67-73	1.5	0.20	0.35	2.06	2.12	2.18	2.24	2.30	2.46	2.56				
				0.49	0.53	0.57	0.59	0.63	0.74	0.79				
				0.98	1.06	1.14	1.18	1.26	1.48	1.58				
				130	**140**	**150**	**160**	**170**	**200**	**220**				
				0.056	0.061	0.065	0.069	0.073	0.087	0.096				
74-80	1.5	0.20	0.40	2.06	2.12	2.18	2.24	2.30	2.46	2.56				
				0.46	0.50	0.52	0.57	0.59	0.68	0.74				
				0.92	1.00	1.04	1.14	1.18	1.36	1.48				
				130	**140**	**150**	**160**	**170**	**200**	**220**				
				0.050	0.054	0.057	0.061	0.065	0.076	0.084				
81-87	1.5	0.20	0.45	2.06	2.12	2.18	2.24	2.30	2.46	2.56				
				0.44	0.46	0.50	0.53	0.56	0.64	0.70				
				0.88	0.92	1.00	1.06	1.12	1.28	1.40				
				130	**140**	**150**	**160**	**170**	**200**	**220**				
				0.047	0.051	0.054	0.058	0.061	0.072	0.080				
88-94	1.5	0.30	0.35	2.04	2.10	2.17	2.23	2.28	2.44	2.54				
				0.46	0.51	0.53	0.55	0.59	0.68	0.75				
				0.92	1.02	1.06	1.10	1.18	1.36	1.50				
				130	**140**	**150**	**160**	**170**	**200**	**220**				
				0.044	0.048	0.051	0.054	0.058	0.068	0.075				
95-101	1.5	0.30	0.40	2.04	2.10	2.17	2.23	2.28	2.44	2.54				
				0.30	0.36	0.41	0.45	0.50	0.65	0.70				
				0.60	0.72	0.82	0.90	1.00	1.30	1.40				
				130	**140**	**150**	**160**	**170**	**200**	**220**				
102-108	1.5	0.30	0.45	0.042	0.045	0.048	0.051	0.054	0.064	0.070				
				2.04	2.10	2.17	2.23	2.28	2.44	2.54				
				0.22	0.27	0.33	0.38	0.42	0.56	0.63				

				0.44	0.54	0.66	0.76	0.84	1.12	1.26
				130	**140**	**150**	**160**	**170**	**200**	**220**
				0.040	0.043	0.047	0.050	0.053	0.062	0.068
109-115	1.5	0.35	0.35	2.03	2.10	2.15	2.21	2.27	2.43	2.53
				0.37	0.43	0.47	0.50	0.53	0.62	0.66
				0.74	0.86	0.94	1.00	1.06	1.24	1.32
				130	**140**	**150**	**160**	**170**	**200**	**220**
				0.038	0.041	0.044	0.046	0.049	0.058	0.064
116-122	1.5	0.35	0.40	2.03	2.10	2.15	2.21	2.27	2.43	2.53
				0.22	0.28	0.32	0.36	0.42	0.54	0.62
				0.44	0.56	0.64	0.72	0.84	1.08	1.24
				130	**140**	**150**	**160**	**170**	**200**	**220**
				0.036	0.038	0.041	0.044	0.046	0.054	0.060
123-129	1.5	0.35	0.45	2.03	2.10	2.15	2.21	2.27	2.43	2.53
				0.14	0.21	0.23	0.30	0.35	0.48	0.54
				0.28	0.42	0.46	0.60	0.70	0.96	1.08

** Estimated values of the free flame height* H_f *for each burner and heat release rate by Heskestad's model [27].*

Table 2 Summary of experimental conditions and results with longitudinal air flow

Test No.	W (m)	D (m)	H (m)	u_a (m/s)	$\sqrt{2\frac{\Delta\rho_f}{\rho_\infty}gH}$ (m/s)	$Q\,(kW)$ Q^{**}(Eq. 10) $\theta\,(degree)$ (Eq. 13) $l_{fe,upstream}\,(m)$ $l_{fe,downstream}\,(m)$ $l_{fe,total}\,(m)$										
1-11	0.5	0.15	0.35	0.6	2.24	**51.0**	**61.2**	**71.4**	**81.6**	**91.8**	**102.0**	**112.2**	**122.4**	**132.6**	**142.8**	**153.0**
						0.111	0.133	0.155	0.177	0.200	0.222	0.244	0.266	0.288	0.310	0.332
						51.9	50.8	50.0	49.2	48.6	48.0	47.4	47.0	46.5	46.0	45.6
						-	-	-	-	-	0.12	0.22	0.30	0.39	0.46	0.48
						-	-	-	-	-	0.17	0.28	0.37	0.47	0.60	0.80
						-	-	-	-	-	0.29	0.50	0.67	0.86	1.06	1.28
12-22	0.5	0.15	0.35	1.2	2.24	**51.0**	**61.2**	**71.4**	**81.6**	**91.8**	**102.0**	**112.2**	**122.4**	**132.6**	**142.8**	**153.0**
						0.111	0.133	0.155	0.177	0.200	0.222	0.244	0.266	0.288	0.310	0.332
						68.6	67.8	67.2	66.6	66.2	65.7	65.3	65.0	64.6	64.3	64.0
						-	-	-	-	-	-	-	-	0.12	0.15	0.22
						-	-	-	-	-	-	-	-	0.32	0.42	0.62
						-	-	-	-	-	-	-	-	0.44	0.57	0.84
23-33	0.5	0.15	0.35	1.8	2.24	**51.0**	**61.2**	**71.4**	**81.6**	**91.8**	**102.0**	**112.2**	**122.4**	**132.6**	**142.8**	**153.0**
						0.111	0.133	0.155	0.177	0.200	0.222	0.244	0.266	0.288	0.310	0.332
						75.3	74.8	74.4	74.0	73.6	73.3	73.0	72.7	72.4	72.2	72.0
						-	-	-	-	-	-	-	-	-	-	0.12
						-	-	-	-	-	-	-	-	-	-	0.16
						-	-	-	-	-	-	-	-	-	-	0.28
34-44	0.5	0.15	0.40	0.6	2.40	**51.0**	**61.2**	**71.4**	**81.6**	**91.8**	**102.0**	**112.2**	**122.4**	**132.6**	**142.8**	**153.0**
						0.127	0.152	0.177	0.203	0.228	0.253	0.279	0.304	0.329	0.355	0.380
						51.9	50.8	50.0	49.2	48.6	48.0	47.4	47.0	46.5	46.0	45.6
						-	-	-	-	-	-	-	-	0.17	0.22	0.30
						-	-	-	-	-	-	-	-	0.28	0.31	0.52
						-	-	-	-	-	-	-	-	0.45	0.53	0.82
45-55	0.5	0.15	0.45	0.6	2.55	**51.0**	**61.2**	**71.4**	**81.6**	**91.8**	**102.0**	**112.2**	**122.4**	**132.6**	**142.8**	**153.0**
						0.142	0.171	0.200	0.228	0.256	0.285	0.313	0.342	0.370	0.400	0.427
						51.9	50.8	50.0	49.2	48.6	48.0	47.4	47.0	46.5	46.0	45.6
						-	-	-	-	-	-	-	-	0.11	0.13	0.23
						-	-	-	-	-	-	-	-	0.30	0.40	0.49
						-	-	-	-	-	-	-	-	0.41	0.53	0.62
56-66	0.5	0.20	0.35	0.6	2.24	**51.0**	**61.2**	**71.4**	**81.6**	**91.8**	**102.0**	**112.2**	**122.4**	**132.6**	**142.8**	**153.0**
						0.083	0.100	0.116	0.133	0.149	0.166	0.182	0.199	0.216	0.232	0.249
						51.9	50.8	50.0	49.2	48.6	48.0	47.4	47.0	46.5	46.0	45.6
						-	-	-	-	-	-	-	0.15	0.21	0.31	0.40
						-	-	-	-	-	-	-	0.20	0.33	0.42	0.58
						-	-	-	-	-	-	-	0.35	0.54	0.53	0.89
67-77	0.5	0.20	0.35	1.2	2.24	**51.0**	**61.2**	**71.4**	**81.6**	**91.8**	**102.0**	**112.2**	**122.4**	**132.6**	**142.8**	**153.0**
						0.083	0.100	0.116	0.133	0.149	0.166	0.182	0.199	0.216	0.232	0.249
						68.6	67.8	67.2	66.6	66.2	65.7	65.3	65.0	64.6	64.3	64.0
						-	-	-	-	-	-	-	-	-	-	0.13
						-	-	-	-	-	-	-	-	-	-	0.29
						-	-	-	-	-	-	-	-	-	-	0.42
78-88	0.5	0.20	0.40	0.6	2.40	**51.0**	**61.2**	**71.4**	**81.6**	**91.8**	**102.0**	**112.2**	**122.4**	**132.6**	**142.8**	**153.0**
						0.077	0.093	0.109	0.124	0.140	0.155	0.171	0.186	0.202	0.218	0.233
						51.9	50.8	50.0	49.2	48.6	48.0	47.4	47.0	46.5	46.0	45.6
						-	-	-	-	-	-	-	-	-	0.15	0.24
						-	-	-	-	-	-	-	-	-	0.27	0.39
						-	-	-	-	-	-	-	-	-	0.42	0.63

						130	**140**	**150**	**160**	**170**	**200**	**220**
						0.053	0.057	0.061	0.065	0.069	0.081	0.089
89-99	1.5	0.25	0.35	0.3	2.24	39.5	37.4	36.1	34.9	33.3	30.8	29.8
						0.14	0.17	0.20	0.24	0.26	0.37	0.43
						0.17	0.20	0.23	0.26	0.29	0.38	0.44
						0.31	0.37	0.43	0.50	0.55	0.75	0.87
100-110	1.5	0.25	0.35	0.5	2.24	**130**	**140**	**150**	**160**	**170**	**200**	**220**
						0.053	0.057	0.061	0.065	0.069	0.081	0.089
						42.9	41.8	40.4	39.4	38.3	36.8	35.8
						-	0.12	0.15	0.20	0.22	0.31	0.37
						-	0.17	0.19	0.23	0.25	0.33	0.41
						-	0.29	0.34	0.43	0.47	0.64	0.75
						130	**140**	**150**	**160**	**170**	**200**	**220**
						0.053	0.057	0.061	0.065	0.069	0.081	0.089
111-121	1.5	0.25	0.35	0.8	2.24	45.7	44.8	43.4	41.9	39.7	37.5	36.8
						-	0.11	0.14	0.18	0.22	0.29	0.35
						-	0.15	0.18	0.21	0.23	0.33	0.38
						-	0.26	0.32	0.39	0.45	0.62	0.73
						130	**140**	**150**	**160**	**170**	**200**	**220**
						0.056	0.061	0.065	0.069	0.073	0.087	0.096
122-132	1.5	0.25	0.40	0.3	2.40	39.5	37.4	36.1	34.9	33.3	30.8	29.8
						0.12	0.15	0.16	0.20	0.23	0.34	0.40
						0.16	0.18	0.18	0.21	0.25	0.35	0.42
						0.28	0.32	0.34	0.41	0.48	0.69	0.82
						130	**140**	**150**	**160**	**170**	**200**	**220**
						0.056	0.061	0.065	0.069	0.073	0.087	0.096
133-149	1.5	0.25	0.40	0.5	2.40	42.9	41.8	40.4	39.4	38.3	36.8	35.8
						-	-	0.11	0.15	0.19	0.28	0.33
						-	-	0.14	0.18	0.22	0.31	0.37
						-	-	0.25	0.33	0.41	0.59	0.70
						130	**140**	**150**	**160**	**170**	**200**	**220**
						0.056	0.061	0.065	0.069	0.073	0.087	0.096
150-156	1.5	0.25	0.40	0.8	2.40	45.7	44.8	43.4	41.9	39.7	37.5	36.8
						-	-	-	0.13	0.16	0.25	0.32
						-	-	-	0.17	0.20	0.29	0.34
						-	-	-	0.30	0.36	0.54	0.66
						130	**140**	**150**	**160**	**170**	**200**	**220**
						0.050	0.054	0.057	0.061	0.065	0.076	0.084
157-163	1.5	0.25	0.45	0.3	2.55	39.5	37.4	36.1	34.9	33.3	30.8	29.8
						-	0.13	0.15	0.18	0.19	0.28	0.34
						-	0.15	0.16	0.18	0.20	0.29	0.35
						-	0.28	0.31	0.36	0.39	0.57	0.69
						130	**140**	**150**	**160**	**170**	**200**	**220**
						0.050	0.054	0.057	0.061	0.065	0.076	0.084
164-170	1.5	0.25	0.45	0.5	2.55	42.9	41.8	40.4	39.4	38.3	36.8	35.8
						-	-	-	-	0.12	0.23	0.29
						-	-	-	-	0.15	0.26	0.32
						-	-	-	-	0.27	0.49	0.61
						130	**140**	**150**	**160**	**170**	**200**	**220**
						0.050	0.054	0.057	0.061	0.065	0.076	0.084
171-177	1.5	0.25	0.45	0.8	2.55	45.7	44.8	43.4	41.9	39.7	37.5	36.8
						-	-	-	-	0.11	0.21	0.27
						-	-	-	-	0.15	0.23	0.30
						-	-	-	-	0.26	0.44	0.57
						130	**140**	**150**	**160**	**170**	**200**	**220**
						0.047	0.051	0.054	0.058	0.061	0.072	0.080
178-184	1.5	0.30	0.35	0.3	2.24	39.5	37.4	36.1	34.9	33.3	30.8	29.8
						0.12	0.14	0.16	0.21	0.25	0.34	0.41
						0.15	0.19	0.21	0.24	0.27	0.37	0.43
						0.27	0.33	0.37	0.45	0.52	0.71	0.84
						130	**140**	**150**	**160**	**170**	**200**	**220**
						0.047	0.051	0.054	0.058	0.061	0.072	0.080
185-191	1.5	0.30	0.35	0.5	2.24	42.9	41.8	40.4	39.4	38.3	36.8	35.8
						-	-	0.11	0.16	0.19	0.28	0.35
						-	-	0.14	0.19	0.22	0.31	0.37
						-	-	0.18	0.23	0.27	0.49	0.61

						130	**140**	**150**	**160**	**170**	**200**	**220**
						0.047	0.051	0.054	0.058	0.061	0.072	0.080
220-226	1.5	0.30	0.35	0.8	2.24	45.7	44.8	43.4	41.9	39.7	37.5	36.8
						-	-	-	0.11	0.15	0.26	0.30
						-	-	-	0.11	0.20	0.29	0.36
						-	-	-	0.22	0.35	0.55	0.66
						130	**140**	**150**	**160**	**170**	**200**	**220**
						0.044	0.048	0.051	0.054	0.058	0.068	0.075
227-233	1.5	0.30	0.40	0.3	2.40	39.5	37.4	36.1	34.9	33.3	30.8	29.8
						-	-	-	0.14	0.19	0.29	0.35
						-	-	-	0.21	0.23	0.31	0.37
						-	-	-	0.35	0.42	0.60	0.72
						130	**140**	**150**	**160**	**170**	**200**	**220**
						0.044	0.048	0.051	0.054	0.058	0.068	0.075
234-240	1.5	0.30	0.40	0.5	2.40	42.9	41.8	40.4	39.4	38.3	36.8	35.8
						-	-	-	-	-	0.20	0.27
						-	-	-	-	-	0.31	0.37
						-	-	-	-	-	0.51	0.64
						130	**140**	**150**	**160**	**170**	**200**	**220**
						0.044	0.048	0.051	0.054	0.058	0.068	0.075
241-247	1.5	0.30	0.40	0.8	2.40	45.7	44.8	43.4	41.9	39.7	37.5	36.8
						-	-	-	-	-	0.14	0.19
						-	-	-	-	-	0.22	0.28
						-	-	-	-	-	0.36	0.47
						130	**140**	**150**	**160**	**170**	**200**	**220**
						0.042	0.045	0.048	0.051	0.054	0.064	0.070
248-254	1.5	0.30	0.45	0.3	2.55	39.5	37.4	36.1	34.9	33.3	30.8	29.8
						-	-	-	0.11	0.15	0.23	0.29
						-	-	-	0.15	0.18	0.27	0.35
						-	-	-	0.26	0.31	0.50	0.64
						130	**140**	**150**	**160**	**170**	**200**	**220**
						0.042	0.045	0.048	0.051	0.054	0.064	0.070
255-261	1.5	0.30	0.45	0.5	2.55	42.9	41.8	40.4	39.4	38.3	36.8	35.8
						-	-	-	-	-	0.14	0.19
						-	-	-	-	-	0.22	0.28
						-	-	-	-	-	0.36	0.47
						130	**140**	**150**	**160**	**170**	**200**	**220**
						0.042	0.045	0.048	0.051	0.054	0.064	0.070
262-268	1.5	0.30	0.45	0.8	2.55	45.7	44.8	43.4	41.9	39.7	37.5	36.8
						-	-	-	-	-	0.12	0.20
						-	-	-	-	-	0.20	0.25
						-	-	-	-	-	0.32	0.45
269-275	1.5	0.35	0.35	0.3	2.24	**130**	**140**	**150**	**160**	**170**	**200**	**220**
						0.040	0.043	0.047	0.050	0.053	0.062	0.068
						39.5	37.4	36.1	34.9	33.3	30.8	29.8
						-	0.12	0.15	0.20	0.23	0.31	0.37
						-	0.16	0.20	0.22	0.24	0.34	0.40
						-	0.28	0.35	0.42	0.50	0.65	0.77
						130	**140**	**150**	**160**	**170**	**200**	**220**
						0.040	0.043	0.047	0.050	0.053	0.062	0.068
276-282	1.5	0.35	0.35	0.5	2.24	42.9	41.8	40.4	39.4	38.3	36.8	35.8
						-	-	-	0.15	0.18	0.26	0.32
						-	-	-	0.17	0.22	0.30	0.35
						-	-	-	0.15	0.26	0.44	0.57
						130	**140**	**150**	**160**	**170**	**200**	**220**
						0.040	0.043	0.047	0.050	0.053	0.062	0.068
283-289	1.5	0.35	0.35	0.8	2.24	45.7	44.8	43.4	41.9	39.7	37.5	36.8
						-	-	-	-	0.14	0.23	0.28
						-	-	-	-	0.19	0.27	0.33
						-	-	-	-	0.33	0.50	0.61
						130	**140**	**150**	**160**	**170**	**200**	**220**
						0.038	0.041	0.044	0.046	0.049	0.058	0.064
299-305	1.5	0.35	0.40	0.3	2.40	39.5	37.4	36.1	34.9	33.3	30.8	29.8
						-	-	-	-	0.13	0.23	0.29
						-	-	-	-	0.20	0.30	0.34
						-	-	-	-	0.33	0.53	0.63

						130	**140**	**150**	**160**	**170**	**200**	**220**
						0.038	0.041	0.044	0.046	0.049	0.058	0.064
306-312	1.5	0.35	0.40	0.5	2.40	42.9	41.8	40.4	39.4	38.3	36.8	35.8
						-	-	-	-	-	0.17	0.24
						-	-	-	-	-	0.24	0.29
						-	-	-	-	-	0.40	0.53
						130	**140**	**150**	**160**	**170**	**200**	**220**
						0.038	0.041	0.044	0.046	0.049	0.058	0.064
313-319	1.5	0.35	0.40	0.8	2.40	45.7	44.8	43.4	41.9	39.7	37.5	36.8
						-	-	-	-	-	0.15	0.21
						-	-	-	-	-	0.20	0.26
						-	-	-	-	-	0.35	0.47
						130	**140**	**150**	**160**	**170**	**200**	**220**
						0.036	0.038	0.041	0.044	0.046	0.054	0.060
320-326	1.5	0.35	0.45	0.3	2.55	39.5	37.4	36.1	34.9	33.3	30.8	29.8
						-	-	-	-	-	0.21	0.27
						-	-	-	-	-	0.25	0.31
						-	-	-	-	-	0.46	0.58
						130	**140**	**150**	**160**	**170**	**200**	**220**
						0.038	0.041	0.044	0.046	0.049	0.058	0.064
327-333	1.5	0.35	0.45	0.5	2.55	42.9	41.8	40.4	39.4	38.3	36.8	35.8
						-	-	-	-	-	0.14	0.20
						-	-	-	-	-	0.19	0.25
						-	-	-	-	-	0.33	0.45
						130	**140**	**150**	**160**	**170**	**200**	**220**
						0.038	0.041	0.044	0.046	0.049	0.058	0.064
334-340	1.5	0.35	0.45	0.8	2.55	45.7	44.8	43.4	41.9	39.7	37.5	36.8
						-	-	-	-	-	-	0.15
						-	-	-	-	-	-	0.21
						-	-	-	-	-	-	0.36